

Precise control of magnetic fields and optical polarization in a time-orbiting potential trap

A. J. Fallon and C. A. Sackett*

Department of Physics, University of Virginia, Charlottesville, VA 22904

(Dated: January 13, 2022)

A time orbiting potential trap confines neutral atoms in a rotating magnetic field. The rotation of the field can be useful for precision measurements, since it can average out some systematic effects. However, the field is more difficult to characterize than a static field, and it makes light applied to the atoms have a time-varying optical polarization relative to the quantization axis. These problems can be overcome using stroboscopic techniques, where either a radio-frequency field or a laser is applied in pulses that are synchronized to the rotating field. Using these methods, the magnetic field can be characterized with a precision of 10 mG and light can be applied with a polarization error of 5×10^{-5} .

I. INTRODUCTION

Magnetic traps are convenient tools for confining atoms over long time scales. The time-orbiting potential (TOP) technique offers the unique feature that the magnetic field at the center of the trap rotates rapidly in time [1]. Because the time average of their magnetic moment is zero, the trapped atoms have reduced sensitivity to low-frequency environmental fields. This makes TOP traps appealing for many types of precision measurements. Indeed, bias field reversals are a standard feature in measurements such as parity violation [2], electric dipole moment searches [3], and other searches for new physics [4]. The TOP trap provides such reversals naturally and at a high frequency. It is not surprising, then, that TOP traps have been considered for various types of precision measurement [5–8].

However, it is critical for many applications that the bias field be well characterized. Ideally, the field should rotate in a well-defined plane with a constant magnitude and rotation rate. If this is the case, then the time average of the atomic moment will be accurately zero, and it will be possible to predict the instantaneous direction of the moment at any given time. Such characterization can be challenging, because it is usually not possible to place a conventional magnetometer in situ at the location of the atoms. In this paper, we present several methods to address this problem, and show that the magnetic field can be optimized to an accuracy of about 10 mG. We also consider the problem of applying light with a well-characterized polarization to the atoms, and show that even with a rotating bias field, this can be achieved with an accuracy of about 5×10^{-5} .

Our own interest is in the application to tune-out wavelength spectroscopy [9, 10]. In this technique, the trapped atoms are illuminated by a laser beam, and the laser is tuned to a frequency where the ac electric polarizability of the atoms vanishes. By measuring this

frequency precisely, information about the atomic matrix elements can be obtained. Our previous experiments [11] took advantage of the rapid bias field reversal in a TOP trap in order to suppress the vector component of the polarizability, which depends sensitively on the polarization of the applied light. For a new experiment [12], we wish to measure the vector polarizability, so it is necessary to characterize both the trap field and the light polarization. Although the discussion is centered on our particular requirements, we believe that the methods presented will be useful for many types of experiments, since it is often necessary to apply well-characterized light to atoms in a well-known magnetic field.

The paper is organized as follows: Section II describes the TOP trap and characterizes how imperfections can distort the bias field. We present a radio-frequency spectroscopy technique that can be used to characterize the bias field as a function of time, and another technique that uses the motion of atoms in the trap to measure an additional component of the ambient field. Section III describes a method to apply polarized light to the trapped atoms, accounting for imperfection from both the light polarization and the magnetic field direction. Finally, Section VI provides a summary, conclusions, and outlook for further improvement.

II. MAGNETIC FIELD CHARACTERIZATION AND CONTROL

Our apparatus uses a modified TOP configuration. Its implementation and operation have been described previously [8, 13], but we summarize relevant details here. The basic trap is formed by a rotating bias field \mathbf{B}_0 and an oscillating linear quadrupole \mathbf{B}_1 . These support the atoms against gravity in the vertical z direction, and they provide approximately harmonic confinement in z and the transverse direction x . An additional spherical quadrupole \mathbf{B}_2 is applied which oscillates at a different frequency and provides adjustable weak confinement in the longitudinal direction y . Altogether, these fields can

*Email: cas8m@virginia.edu

be expressed as $\mathbf{B}_{tot} = \mathbf{B}_0 + \mathbf{B}_1 + \mathbf{B}_2$ with

$$\mathbf{B}_0 = B_0(\sin \Omega_1 t \hat{x} + \cos \Omega_1 t \hat{z}) \quad (1)$$

$$\mathbf{B}_1 = B'_1(z\hat{z} - x\hat{x}) \cos \Omega_1 t \quad (2)$$

$$\mathbf{B}_2 = B'_2(2y\hat{y} - x\hat{x} - z\hat{z}) \cos \Omega_2 t. \quad (3)$$

The trapping potential is given by $\mu\langle|\mathbf{B}_{tot}|\rangle$, where the angle brackets denote a time average and μ is the magnetic moment of the spin state. Our experiments use the $F = 2, m_F = 2$ hyperfine state of ^{87}Rb , so that μ is approximately equal to the Bohr magneton μ_B . In general the time average must be calculated numerically, but if the atoms remain close to the origin then it is accurate to Taylor expand $|\mathbf{B}_{tot}|$ to second order and perform the time average analytically. The result is

$$\begin{aligned} \langle|\mathbf{B}|\rangle \approx & B_0 - \frac{1}{2}B'_1 z + \left(\frac{3B_1'^2}{16B_0} + \frac{B_2'^2}{4B_0}\right)x^2 \\ & + \frac{B_2'^2}{B_0}y^2 + \left(\frac{B_1'^2}{16B_0} + \frac{B_2'^2}{4B_0}\right)z^2. \end{aligned} \quad (4)$$

Here we assume that Ω_1 and Ω_2 are approximately incommensurate, so that no cross terms survive the time average. Experimentally we use $\Omega_1 = 2\pi \times 12.8$ kHz and $\Omega_2 = 2\pi \times 1$ kHz. Typically we use $B_0 \approx 24$ G and we set $B'_1 \approx 30.7$ G/cm such that the linear term in the TOP potential cancels the gravitational potential mgz . We set $B'_2 \approx 2.5$ G/cm to provide an oscillation frequency $\omega_y \approx 2\pi \times 1$ Hz. The measured ω_x and ω_z confinement frequencies are then approximately $2\pi \times 5.1$ Hz and $2\pi \times 3.3$ Hz, respectively. In comparison, Eq. (4) predicts values of 4.9 and 2.9 Hz. The difference is due to non-uniformity of the bias field B_0 , but this has negligible impact on the work discussed here since it alters the spatial variations of the field but not the field itself at the potential minimum.

A number of other non-idealities do impact the field experienced by the atoms. The rotating bias field components are produced by two separate coils. These coils may not be perfectly orthogonal, their fields may have different amplitudes, and their phase difference may differ from $\pi/2$. In addition a dc background field may be present. All of these effects can introduce time-dependent variations in the field magnitude and direction at the position of the atoms. The goal here is to characterize and control these effects.

The two components of the bias field are produced by long rectangular coils oriented near $\pm 45^\circ$ from vertical. We express these components as

$$\begin{aligned} \mathbf{B}_{0a} = & \frac{B_0}{\sqrt{2}}(1 + \Delta)[(1 + \psi_1)\hat{x} - (1 - \psi_1)\hat{z}] \\ & \times \sin\left(\Omega_1 t - \frac{\pi}{4} + \xi_1\right) \end{aligned} \quad (5)$$

and

$$\begin{aligned} \mathbf{B}_{0b} = & \frac{B_0}{\sqrt{2}}(1 - \Delta)[(1 - \psi_2)\hat{x} + (1 + \psi_2)\hat{z}] \\ & \times \sin\left(\Omega_1 t + \frac{\pi}{4} + \xi_2\right), \end{aligned} \quad (6)$$

where Δ characterizes the amplitude mismatch, the ψ_i are small angular deviations from the ideal orientation, and the ξ_i are phase offsets from the \mathbf{B}_1 quadrupole oscillation. It is useful to define common and differential variables $\psi = (\psi_1 + \psi_2)/2$, $\psi' = (\psi_1 - \psi_2)/2$, $\xi = (\xi_1 + \xi_2)/2$, and $\xi' = (\xi_1 - \xi_2)/2$.

Expanding to first order in these small variables, we find a total bias field of

$$\begin{aligned} \frac{\mathbf{B}_0}{B_0} = & \left[(1 + \xi' + \psi') \sin \Omega_1 t - (\Delta - \xi + \psi) \cos \Omega_1 t\right] \hat{x} \\ & + \left[(1 - \xi' - \psi') \cos \Omega_1 t - (\Delta + \xi - \psi) \sin \Omega_1 t\right] \hat{z}. \end{aligned} \quad (7)$$

To this we add the \mathbf{B}_1 quadrupole field from (2) and an environmental field $\mathbf{B}_E = B_{Ex}\hat{x} + B_{Ey}\hat{y} + B_{Ez}\hat{z}$ with $|B_{Ei}| \ll B_0$. We then calculate the TOP potential using the same time-averaging procedure as before. We omit the B_2 field since it is an order of magnitude smaller than the B_1 quadrupole. The result is

$$\begin{aligned} \langle|\mathbf{B}_{tot}|\rangle = & B_0 \left\{ 1 + \frac{1}{4}(\Delta - 2\xi + 2\psi)qx + \frac{1}{4}(2 - \xi' - \psi')qz \right. \\ & \left. + \frac{3}{16}q^2x^2 + \frac{1}{16}q^2z^2 \right\}, \end{aligned} \quad (8)$$

with $q \equiv B'_1/B_0$. Here we keep terms to first order in $\Delta, \psi, \psi', \xi, \xi'$, and B_{Ei}/B_0 , except in the x^2 and z^2 terms where the non-idealities are omitted.

The atoms will be trapped at the minimum of the total potential. Along x the minimum can be found directly as

$$x_0 = -\frac{2(\Delta - 2\xi + 2\psi)}{3q}. \quad (9)$$

We take the vertical position z_0 as an independent parameter. We can then express the time-dependent field magnitude at the center, to first order in non-idealities, as

$$\begin{aligned} |\mathbf{B}_{tot}|(t) = & B_0 \left\{ 1 + \frac{1}{2}qz_0 + q_{Ex} \sin \Omega_1 t + q_{Ez} \cos \Omega_1 t \right. \\ & + \frac{1}{2}(qz_0 - 2\xi' - 2\psi') \cos 2\Omega_1 t \\ & \left. - \frac{2}{3}(\Delta + \xi - \psi) \sin 2\Omega_1 t \right\} \end{aligned} \quad (10)$$

with $q_{Ei} = B_{Ei}/B_0$. We see that the non-idealities combine to give oscillating contributions to $|\mathbf{B}|$ that have different frequencies and phases. Measuring these different components therefore provides information about

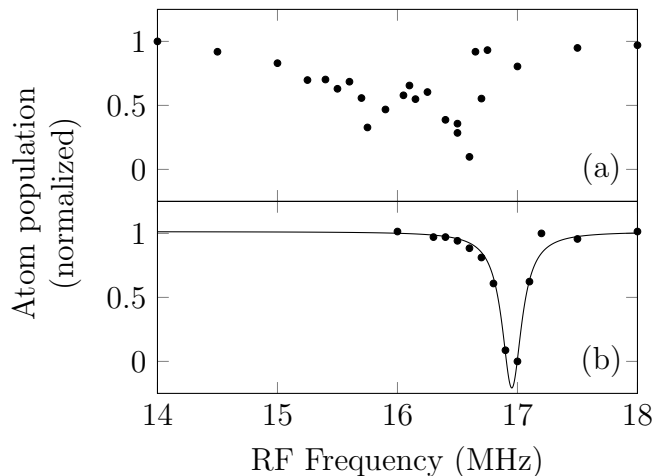


FIG. 1: Radio-frequency spectra of trapped condensate atoms. The vertical axis shows the fraction of atoms remaining in the trap after rf is applied at the indicated frequency. (a) Spectrum obtained using a single long pulse of duration 200 ms. (b) Spectrum obtained using a train of 250 pulses each with 10 μ s duration. The pulses are synchronized to the 12.8 kHz bias rotation frequency, so that the magnetic field has the same value during each pulse. At the delay time shown, the field magnitude happens to take on nearly its largest value. The curve is a Lorentzian fit.

the non-idealities, which can then be compensated with the goal of producing a bias field that varies as little as possible. We see that it is not necessary for all the non-ideal parameters to be zero, since the combinations $qz_0 - 2\xi' - 2\psi'$ and $\Delta + \xi - \psi$ appear together. As long as the parameters are adjusted to make $|\mathbf{B}_{tot}|$ constant in time, the net bias field will rotate uniformly as

$$\mathbf{B}_{tot} = B_0 \left(1 + \frac{qz_0}{2}\right) (\hat{x} \sin \Omega_1 t + \hat{z} \cos \Omega_1 t) + B_{Ey} \hat{y}. \quad (11)$$

The amplitude shift due to z_0 is typically unimportant, so we do not attempt to measure or compensate for it.

Information about the magnetic field at the location of the atoms can be obtained by driving the Zeeman transition $m_F = 2 \rightarrow m_F = 1$ using a radio-frequency field. Atoms making the transition are no longer supported against gravity and fall out of the trap. If the atoms form a Bose-Einstein condensate, the thermal broadening of the rf spectrum will be negligible and the character of the spectrum will be determined entirely by the variations in the magnetic field at the trap potential minimum. Figure 1(a) shows the spectrum observed when a continuous rf pulse is applied to an unoptimized trap. The broad and complicated lineshape indicates that the atoms experience considerable variations in the trap field, making the resonant frequency vary over the course of the TOP period.

More detailed information can be obtained by applying a pulsed rf field, with the pulses synchronized to the Ω_1 trap frequency. In this way we obtain a snap-shot of the

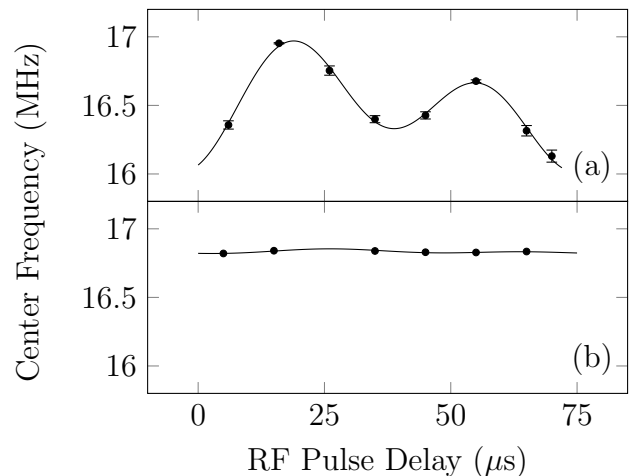


FIG. 2: Time-dependence of the magnetic field magnitude during TOP field oscillation, as measured by the center frequency of spectra such as in Fig. 1(b). Error bars are one- σ errors from the fit. Solid curves are fits to the form of Eq. (10). (a) Initial variation in a trap using nominal driver current amplitudes. (b) Variation after adjusting the oscillating terms in (10) to be zero. The residual oscillation corresponds to field variations of less than 10 mG.

field value at a particular point in the cycle, using the same principle as the stroboscope. Figure 1(b) shows the spectrum obtained with a 10 μ s pulse duration at a fixed delay with respect to the 80 μ s oscillation period. The spectrum is much narrower, with a width close to the 60 kHz transform limit of the pulse. The frequency at which the peak occurs indicates the instantaneous value of the field at that time.

To map out the field amplitude as a function of time, we take a series of spectra such as Fig. 1(b) with different time delays between the trap current oscillation and the rf pulses. A typical result is shown in Fig. 2(a). We fit such data to a function with the form of Eq. (10), where the amplitudes of each term are fit parameters. The solid line in the figure shows the result, which generally fits the data well.

The fitted coefficients indicate how the parameters B_{Ex} , B_{Ez} , q and Δ can be adjusted to make $|\mathbf{B}|$ constant in time. We do not adjust the ψ_i or ξ_i variables. The environmental fields are controlled using a set of bias coils, while q and Δ are set by the quadrupole and bias current amplitudes respectively. Figure 2(b) shows a spectral measurement of the field variations after the oscillating components have been minimized, showing that the transition frequency remains nearly constant during the bias rotation. Our measurement resolution is 5 mG, and we are able to zero each frequency component to that level. This corresponds to a total rms field variation of about 10 mG.

The rf spectroscopy technique is insensitive to the B_{Ey} component, since it makes only a dc contribution to the field magnitude. However, we want to ensure that the

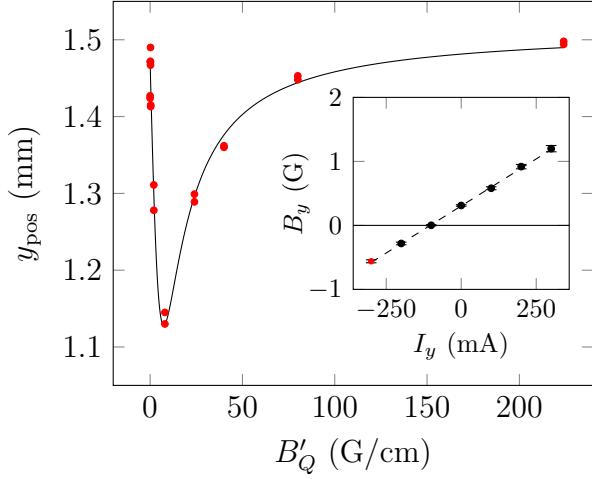


FIG. 3: Using trap motion to determine the B_{Ey} background field. In the main graph, data points are the observed trap positions as the dc gradient B'_Q is slowly varied. The curve is a fit to Eq. (14) yielding $B_{Ey} = 0.56(2)$ G. The inset shows measured B_{Ey} values as a function of current I_y through a pair of dc bias coils. The red point corresponds to the data in the main graph.

field rotates in the xz plane, so it is necessary to determine and null out the B_{Ey} field as well. A way to achieve this is by applying a dc spherical quadrupole field

$$\mathbf{B}_Q = B'_Q(2z\hat{z} - x\hat{x} - y\hat{y}) \quad (12)$$

to the atoms in the TOP trap. We focus on the resulting confinement potential along the y direction, taking $x = z = 0$. Calculation of the time-averaged field magnitude as in Eq. (8) yields

$$\langle |\mathbf{B}| \rangle = B_0 + \frac{B_2'^2}{B_0} y^2 + \frac{B_Q'^2}{2B_0} (y - y_E)^2, \quad (13)$$

where $y_E \equiv B_{Ey}/B'_Q$ is the position where the net dc field is zero. The minimum of the resulting potential occurs at position

$$y_0 = y_E \frac{B_Q'^2}{B_Q'^2 + 2B_2'^2} = \frac{B_{Ey} B'_Q}{B_Q'^2 + 2B_2'^2}. \quad (14)$$

To find B_{Ey} , we measure the condensate's position while varying B'_Q and fit the results to Eq. (14). Typical data are shown in Fig. 3(a), along with the fit curve. Figure 3(b) shows the values of B_{Ey} obtained from the fit as current through a dc bias coil is varied. The slope of the curve is consistent with the bias coil geometry, and the intercept allows us to determine where B_{Ey} is zero to an accuracy of 7 mG. We used a similar technique observing motion along the z direction, and verified that the trap motion and rf spectroscopy techniques give consistent results for the B_{Ez} component.

The background magnetic fields and rotating bias field show good stability over long timescales without the

need for regular adjustments. We observed drifts of less than 10 mG over several months of operation. However, the linear quadrupole amplitude B'_1 does drift by about 30 mG/cm over the course of days, making regular adjustments necessary. It is easy to see when B'_1 has shifted, because the z position of the atoms changes.

III. OPTICAL POLARIZATION CHARACTERIZATION AND CONTROL

In addition to having a well-controlled magnetic field, we need to apply a light field with a well known and stable polarization. This is a critical element for our tune-out wavelength studies, and it is important for other precision measurements as well. For our experiments, we need to apply σ_+ polarized light to the atoms with a polarization accuracy better than 10^{-4} .

Two factors make polarization control challenging here. The first is that the bias field at the atoms is rotating, so relative to the quantization axis the light polarization is constantly changing. This can be addressed using the same technique described above for rf spectroscopy, by applying short pulses of light that are synchronous with the magnetic field oscillations. If light polarization $\hat{\mathcal{E}}$ is applied to the atoms, the polarization fidelity can be defined as $F = \langle |\hat{\mathcal{E}}^* \cdot \hat{\sigma}_+|^2 \rangle$, where the angle brackets denote a time average over the direction of the field. We use circularly polarized light travelling along z , with $\hat{\mathcal{E}} = (\hat{x} - i\hat{y})/\sqrt{2}$. The direction of the trap field determines the $\hat{\sigma}_+$ vector as $(\hat{x}' - i\hat{y}')/\sqrt{2}$, for $\hat{x}' = \cos\Omega_1 t \hat{x} + \sin\Omega_1 t \hat{z}$. If the light applied for time $\tau \ll 1/\Omega_1$, centered on $t = 0$, then the time-averaged fidelity is

$$F = 1 - \frac{1}{48} \Omega_1^2 \tau^2. \quad (15)$$

For $\Omega_1 = 2\pi \times 12.8$ kHz, this gives a negligible polarization error of 2×10^{-6} at a pulse duration of 120 ns.

The second challenging factor is that optical polarizing elements are not ideal, so the light polarization reaching the atoms will not be perfect. For instance, stress-induced birefringence of the vacuum window introduces polarization errors that are difficult to determine in situ [14]. Similarly, waveplate retardances are not exact and can vary with temperature and light wavelength.

The behavior of the polarization can be characterized using the Stokes vector $[S_1, S_2, S_3]$, which can be related to the left- and right-circular polarized electric field components \mathcal{E}_ℓ and \mathcal{E}_r by $S_1 = 2\text{Re}(\mathcal{E}_r \mathcal{E}_\ell^*)$, $S_2 = -2\text{Im}(\mathcal{E}_r \mathcal{E}_\ell^*)$ and $S_3 = |\mathcal{E}_r|^2 - |\mathcal{E}_\ell|^2$. The S_0 Stokes parameter is here taken to be unity, and we normalize $S_1^2 + S_2^2 + S_3^2 = |\mathcal{E}_r|^2 + |\mathcal{E}_\ell|^2 = 1$. When the laser beam passes through a birefringent element with retardance δ

and axis at angle α , the effect on \mathbf{S} is given by the Mueller matrix [15]

$$M(\alpha, \delta) = \begin{bmatrix} \cos^2 2\alpha + \sin^2 2\alpha \cos \delta & \cos 2\alpha \sin 2\alpha (1 - \cos \delta) & \sin 2\alpha \sin \delta \\ \cos 2\alpha \sin 2\alpha (1 - \cos \delta) & \cos^2 2\alpha \cos \delta + \sin^2 2\alpha & -\cos 2\alpha \sin \delta \\ -\sin 2\alpha \sin \delta & \cos 2\alpha \sin \delta & \cos \delta \end{bmatrix}, \quad (16)$$

such that input \mathbf{S} is transformed to $\mathbf{S}' = M\mathbf{S}$. The fidelity of the output polarization with respect to the initial state is given by

$$F = \frac{1}{2} (1 + \mathbf{S}' \cdot \mathbf{S}). \quad (17)$$

In the case of weak birefringence $\delta \ll 1$, the fidelity can be calculated to second order as

$$F \approx 1 - \frac{\delta^2}{4} [(S_1 \sin 2\alpha - S_2 \cos 2\alpha)^2 + S_3^2], \quad (18)$$

The error is zero for linearly polarized light aligned to the axis of the retarder, but in general the fidelity decreases by a factor of order δ^2 . A similar error occurs for light passing through a waveplate if δ is interpreted as the birefringence error and \mathbf{S} is the ideal output polarization. We observe typical values of δ to be 5×10^{-2} or greater, which imposes a polarization error on the order of 10^{-3} . It is therefore necessary to correct for these errors.

We prepare the polarization state starting with linear polarization produced by a Glan–Taylor polarizer, with an estimated error below 10^{-5} [16]. The conversion to circular polarization is achieved using a Fresnel rhomb, which is the most stable retarder readily available [17]. Using BK7 glass, the calculated wavelength variation of the retardance is below 10^{-8} rad/nm, and the calculated temperature dependence is about 4×10^{-6} rad/K. We verified experimentally that the retardance of the rhomb is stable at our measurement sensitivity of 10^{-5} .

The retardance of the rhomb is not easily adjustable, so prior to the rhomb we pass the light through two Meadowlark Optics zero-order polymer retarders, one a quarter-wave plate and the other a half-wave plate. Both plates are aligned with their axes close to the incident polarization axis, which limits the sensitivity to retardance errors or drifts. The polarization state exiting the rhomb is then

$$\mathbf{S}_{\text{rhomb}} = \begin{bmatrix} -2\alpha_1 \\ 4\alpha_2 - 2\alpha_1 \\ 1 \end{bmatrix} + O(\alpha^2) \quad (19)$$

where α_1 is the angle of the quarter-wave plate and α_2 the angle of the half-wave plate. Any inaccuracies of the rhomb or polarization shifts from subsequent optical elements will give additional small contributions to S_1 and S_2 . We see, however that the two waveplate angles provide sufficient degrees of freedom to compensate for

any such contributions, allowing S_1 and S_2 to be tuned to zero.

It is useful to calculate the projection of the light polarization onto the atomic σ_- and π components, in terms of the Stokes parameters and the relative orientation between the laser beam and the magnetic field. The results are

$$|\mathcal{E}_\pi|^2 = \frac{1}{2} (1 + S_1 \cos 2\phi + S_2 \sin 2\phi) \sin^2 \theta \approx \frac{\theta^2}{2} \quad (20)$$

$$|\mathcal{E}_-|^2 = \frac{1}{2} (1 - S_3 \cos \theta) - \frac{1}{4} (1 + S_1 \cos 2\phi + S_2 \sin 2\phi) \sin^2 \theta \approx \frac{S_1^2 + S_2^2}{4}, \quad (21)$$

where the laser beam propagates at polar angles (θ, ϕ) with respect to the field. We see that the π polarization component depends primarily on alignment, while the σ_- term is set by the polarization optics. The polarization error $1 - F$ can be expressed here as $|\mathcal{E}_\pi|^2 + |\mathcal{E}_-|^2$.

This analysis shows that in order to apply pure σ_+ light to the atoms, several conditions must be met. First, the laser beam should be aligned to the z direction of the trap. Second, the laser pulse timing must be set so that the pulse center arrives when the trap field points along z . Finally, the waveplate angles α_1 and α_2 must be adjusted to compensate for the birefringence of the vacuum window and any other polarization errors.

In order to set these values precisely, we require a means to characterize the polarization at the location of the atoms. As shown in Fig. 4, our ^{87}Rb atoms are trapped in the $F = 2, m_F = 2$ ground state, and we measure the polarization fidelity by tuning the laser to the $5P_{1/2} F = 2$ level. This level has no state with angular momentum projection $m = 3$, so pure σ_+ light does not scatter from the atoms. We can then use the scattering rate as a measure of polarization error, which is very sensitive since scattering even a single photon causes an atom to be removed from a Bose–Einstein condensate.

To make the measurement, we apply up to 4000 light pulses, each of duration 120 ns and with a period of $2\pi/\Omega_1$. We then measure the fraction of atoms remaining in the trap. We observe the scattering rate for near- σ_+ light to be a complicated function of the total intensity, as seen in Fig. 5(a). This is due to the formation of a dark state. For example, Fig. 4 shows a case where a small amount of π light is present. This excites atoms into the $m' = 2$ state, where they can decay to the $m = 1$ ground

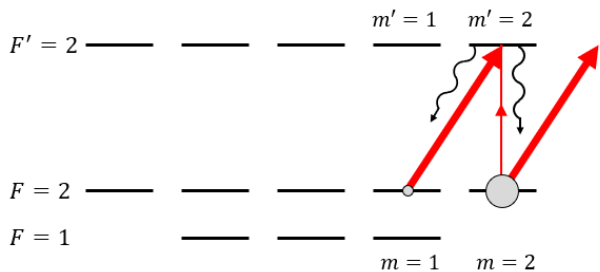


FIG. 4: Level diagram for polarization testing. Atoms are trapped in the $F=2, m=2$ state, where they cannot scatter σ_+ polarized light. Any contamination by π or σ_- light does lead to scattering and loss from the trap; the diagram shows π light for illustration. Because of the scattering, a small population can be temporarily established in the $F=2, m=1$ state, where the strong excitation to $m'=2$ can destructively interfere with the excitation amplitude from $m=2$. This leads to a suppression of scattering at high optical intensity.

state and eventually fall out of the trap. However, the atoms do not move significantly during the short laser pulse, so atoms with $m=1$ undergo a strong excitation to the $m'=2$ excited state from the σ_+ light. For the proper spin superposition $|\psi\rangle = \sum c_i |m_i\rangle$, the excitation amplitude from $m=1$ to $m'=2$ can cancel the amplitude from $m=2$ to $m'=2$, leaving the state $|\psi\rangle$ dark.

The trapped atoms experience a Zeeman splitting of about 17 MHz, as seen in Fig. 2. This causes the phases in $|\psi\rangle$ to change in time, so in order to maintain the dark state it is necessary for the optical Rabi frequency of the light to be comparable to the Zeeman splitting. This corresponds to an intensity I of roughly ten times the saturation intensity I_S , which agrees with the measured intensity where the atom loss starts to level out. The Zeeman shift causes substantial dephasing during the 80 μ s between laser pulses, and measurements confirm that that each pulse has an independent effect on the atoms.

We have analyzed the formation of the dark state by solving the optical Bloch equations for the thirteen relevant atomic states involved [18]. This includes the $F=2$ ground states, the $F'=2$ excited states, and the $F=1$ ground states which can be populated by spontaneous emission. We model the evolution during a single pulse of the light, and determine the fraction of atoms ϵ lost from the initial $m=2$ state as a function of the intensity components I_i , with $I_\pi, I_- \ll I_+$. Figure 5(b) shows how the loss depends on the total intensity, and the shape of the curve agrees reasonably well with the experimental observations. We do not clearly observe the predicted oscillations at high intensity, but it is likely they are washed out by experimental intensity noise. The inset shows that the loss ϵ depends linearly on the polarization impurity.

The formation of the dark state limits the sensitivity of our polarization measurement, since we cannot arbitrarily increase the laser intensity without saturating the loss rate. Instead we experimentally adjust the intensity

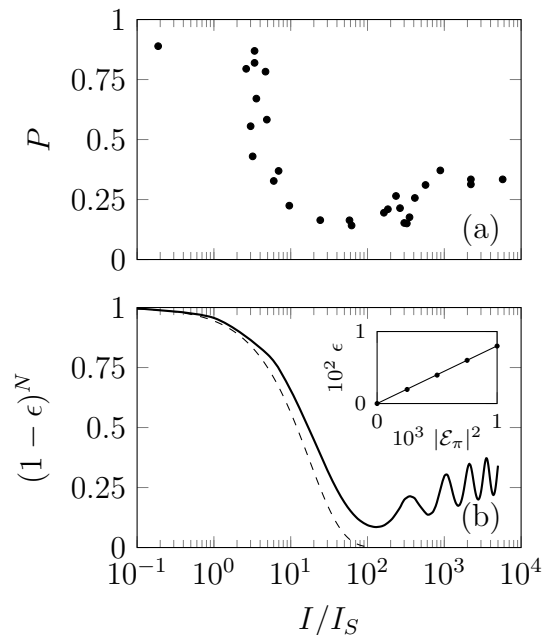


FIG. 5: (a) Experimental measurements of atom loss. Data points show the fraction of atoms P remaining in the trap after 1280 pulses of laser light at the indicated total intensity, relative to the saturation intensity I_S . (b) Numerical calculation of the survival probability after N pulses $(1-\epsilon)^N$ for $N=1280$. The solid curve shows the result from the optical Bloch equations for a polarization impurity $\mathcal{E}_\pi = 2 \times 10^{-4}$. The dashed curve shows the behavior that would be expected in the absence of dark-state formation. The inset shows that the loss ϵ depends linearly on the polarization impurity, here calculated at $I=100I_S$. The slope $d\epsilon/d|\mathcal{E}_\pi|^2$ is approximately 9.5 at the first minimum.

to locate the value where the loss rate is largest, and then use the Bloch equation model to determine the polarization impurity corresponding to the measured loss. This calibration depends differently on the π and σ_- components, with the loss rate always being greater for σ_- light. For both polarizations, the loss rate maximum occurs at $I \approx 100I_S$. At that minimum we evaluate the loss per pulse as $\epsilon = \kappa_i |\mathcal{E}_i|^2$, finding $\kappa_\pi \approx 9.5$ and $\kappa_- \approx 18$. To be conservative, we assume that the impurity is all π light to set an upper bound. We are then able to relate the measured atom survival probability $P = (1-\epsilon)^N$ to the polarization impurity $|\mathcal{E}_\pi|^2$ via

$$|\mathcal{E}_\pi|^2 = \frac{1 - P^{1/N}}{\kappa_\pi}, \quad (22)$$

for number of pulses N . For the data of Fig. 5(a), we obtain $|\mathcal{E}_\pi|^2 \approx 1.5 \times 10^{-4}$.

Following this procedure, we can optimize the light polarization, pulse timing, and beam direction to minimize the polarization error. For example, Fig. 6 shows how the atom loss varies when the delay time of the light pulse is changed. This corresponds to varying the angle between the beam and the rotating field, with

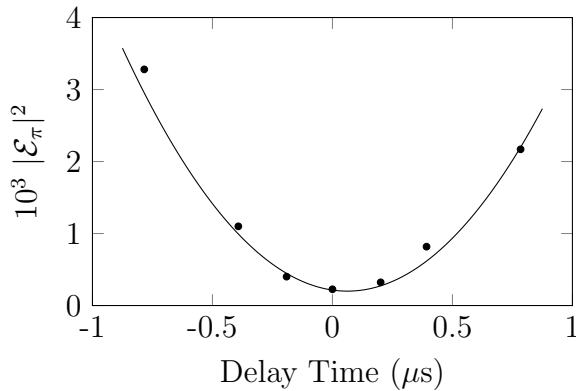


FIG. 6: Dependence of polarization error on beam alignment. Points show the fraction of π polarized light at the atoms, determined as described in the text. The angle θ between the laser beam and the rotating field is varied by adjusting the time t at which the light pulse is centered. The curve is a parabolic fit giving $|\mathcal{E}_\pi|^2 = 0.61(3) \cdot \Omega_1^2 t^2$, in reasonable agreement with the expectation $|\mathcal{E}_\pi|^2 = \theta^2/2$.

$\Delta\theta = \Omega_1 \Delta t$. The polarization error varies like $\theta^2/2$, as expected. The optimum delay time corresponds to the minimum of the curve. After optimizing all parameters in this way, we consistently obtain a loss rate corresponding to $|\mathcal{E}_\pi|^2 = 5 \times 10^{-5}$. Alternatively, if we assume the polarization impurity to be σ_- , we infer $|\mathcal{E}_-|^2 = 3 \times 10^{-5}$.

To confirm this result, we reversed the handedness of the light by rotating the initial polarizer by 90° , and offset the pulse timing by a half-period π/Ω_1 . We then re-optimized the waveplate angles but did not otherwise change the timing or beam pointing direction. We found that the same level of polarization error was obtained. This also verifies the procedures used to zero the B_{Ex} and B_{Ey} environmental field components, since it shows that the bias field does in fact reverse direction after a half period.

IV. CONCLUSION

Using the methods discussed above, we have demonstrated control of the magnetic field in a TOP trap with 10 mG precision, and we have demonstrated the ability to apply polarized light to the trapped atoms with errors below 10^{-4} . These values are sufficient for our proposed tune-out wavelength experiments, but we briefly discuss here how much more improvement is possible.

In the case of the rf spectroscopy technique, the sensitivity is fundamentally limited by the rf pulse duration. To measure frequencies of $2\Omega_1$, the maximum usable pulse duration is a quarter period. At our TOP frequency, this gives a Fourier-limited bandwidth of 30 kHz. It is reasonable to measure the line center to 1% of the width, but beyond that it will likely be necessary to develop a more complex model accounting for effects like

non-uniformity of the bias field, non-idealities of the rf pulse, and effects of the B_2 field. At a line-splitting accuracy of 1%, the 300 Hz frequency resolution corresponds to $\delta B = 0.4$ mG.

The trap position method is limited by the ability to measure the position of the Bose condensate. As the dc quadrupole B'_Q is varied, the maximum atom displacement is $\delta y = 2^{-3/2} B_{Ey}/B'_2$. If B'_2 gradient is made too small, then it is difficult to ensure the atoms adiabatically follow the trap bottom as B'_Q changes, but a reduction to $B'_2 \approx 1$ G/cm is reasonable. At that confinement, the Thomas-Fermi size of the condensate along y would be $50 \mu\text{m}$, and it is feasible to measure the condensate position with an accuracy of about $5 \mu\text{m}$. The corresponding uncertainty in B_{Ey} is then about 1 mG. We conclude that, overall, it should be possible to reach a performance level for the magnetic field at the mG level without dramatic changes to the measurement techniques presented here. It would be relatively straightforward to reduce the B_E environmental fields further using magnetic shielding techniques.

Static magnetic traps can achieve field stabilities of $10 \mu\text{G}$ [19]. This is well below the variations we achieve, although we expect the time-varying components of our field to have comparable amplitude stability [20]. We expect a TOP trap will be attractive for experiments where the benefits of the rapid field rotation outweigh the impacts of the corresponding mG-level variations.

The ultimate limit on the polarization accuracy is harder to assess. One limitation is scattered light from optics and vacuum windows, which can be challenging to suppress at the 10^{-6} level. Another limit is set by the spatial uniformity of the retardance. Stress-induced birefringence is typically non-uniform [14], and retardance variations of a few mrad across the laser beam would limit the polarization purity to 10^{-5} . If an optic has a peak retardance of tens of mrad that varies on the cm scale, then the variations could be significant for a mm-diameter laser beam. To our knowledge, the polarization errors demonstrated here are comparable to what is typically achieved in a static magnetic trap.

In summary, we have demonstrated techniques to optimize the magnetic field and light polarization in a TOP trap, reaching accuracies of 10 mG and 10^{-4} respectively. These techniques will be important for our own proposed tune-out wavelength measurements, but we hope that they will also be of use for other experiments that could benefit from the special features of the TOP trap.

Acknowledgments

This work was supported by the National Science Foundation (Grant No. PHY-1607571). We are grateful to Seth Berl for coding support and to Eddie Moan for helpful conversations and comments on the manuscript.

-
- [1] W. Petrich, M. H. Anderson, J. R. Ensher, and E. A. Cornell, *Phys. Rev. Lett.* **74**, 3352 (1995).
 - [2] M. L. J. Guéna and M.-A. Bouchiat, *Mod. Phys. Lett. A* **20**, 375 (2005).
 - [3] T. E. Chupp, P. Fierlinger, M. J. Ramsey-Musolf, and J. T. Singh, *Rev. Mod. Phys.* **91**, 015001 (2019).
 - [4] M. S. Safronova, D. Budker, D. DeMille, D. F. J. Kimball, A. Derevianko, and C. W. Clark, *Rev. Mod. Phys.* **90**, 025008 (2018).
 - [5] S. G. Crane, S. J. Brice, A. Goldschmidt, R. Guckert, A. Hime, J. J. Kitten, D. J. Vieira, and X. Zhao, *Phys. Rev. Lett.* **86**, 2967 (2001).
 - [6] A. S. Arnold, *J. Phys. B: At. Mol. Opt. Phys.* **37**, L29 (2004).
 - [7] S. Gupta, K. W. Murch, K. L. Moore, T. P. Purdy, and D. M. Stamper-Kurn, *Phys. Rev. Lett.* **95**, 143201 (2005).
 - [8] J. M. Reeves, O. Garcia, B. Deissler, K. L. Baranowski, K. J. Hughes, and C. A. Sackett, *Phys. Rev. A* **72**, 051605 (2005).
 - [9] L. J. LeBlanc and J. H. Thywissen, *Phys. Rev. A* **75**, 053612 (2007).
 - [10] B. Arora, M. S. Safronova, and C. W. Clark, *Phys. Rev. A* **84**, 043401 (2011).
 - [11] R. H. Leonard, A. J. Fallon, C. A. Sackett, and M. S. Safronova, *Phys. Rev. A* **92**, 052501 (2015).
 - [12] A. Fallon and C. Sackett, *Atoms* **4** (2016), [10.3390/atoms4020012](https://doi.org/10.3390/atoms4020012).
 - [13] J. H. T. Burke, *Improvements and applications of a guided wave Bose-Einstein condensate interferometer*, Ph.D. thesis, University of Virginia (2010).
 - [14] Schott Advanced Optics, *Stress in optical glass*, Tech. Rep. TIE-27 (SCHOTT AG, 2019).
 - [15] R. A. Chipman, “Handbook of optics,” (McGraw-Hill, New York, 2010) Chap. 15, 3rd ed.
 - [16] Y. Takubo, N. Takeda, J. H. Huang, K. Muroo, and M. Yamamoto, *Meas. Sci. Technol.* **9**, 20 (1998).
 - [17] J. M. Bennett, *App. Opt.* **9**, 2123 (1970).
 - [18] C. Foot, *Atomic Physics* (Oxford University Press, 2005).
 - [19] C. J. Dedman, R. G. Dall, L. J. Byron, and A. G. Truscott, *Review of Scientific Instruments* **78**, 024703 (2007), <https://doi.org/10.1063/1.2472600>.
 - [20] K. L. Baranowski and C. A. Sackett, *J. Phys. B: At. Mol. Opt. Phys.* **39**, 2949 (2006).